Coherent Imaging of Etched Fission Fragments and Alpha Particles Tracks in a CR-39 SSNTD

Moses J. Eghan[1,*], Osborn C. Oppon[2], Kofi B. Nyarko[3] and Paul K. Buah-Bassuah[1]
[1] *Laser and Fiber Optics Centre, Department of Physics, University of Cape Coast, Cape Coast, Ghana*
[2] *National Nuclear Research Institute, Ghana Atomic Energy Commission, , Legon, Accra, Ghana*
[3]*Department of Geography and Tourism, University of Cape Coast, Cape Coast, Ghana*

CR-39 SSNTD detects radioactive emissions and by etching provides a means of studying tracks of emitted particles such as Fission Fragments and alpha particles. A new way of imaging etched fission fragments and alpha tracks in CR-39 detector is presented. A commercial software Image Pro Plus is used in digitizing the images, counting and classifying the tracks. Variations of etched track dimensions with particle energies are presented.

1. Introduction

The apparent applications of Solid-State Nuclear Track Detectors (CR-39 SSNTD) in the last decade have presented the need to develop techniques to image large detectors areas, count and quantify track parameters in the least possible time. The evaluation of these tracks in CR-39 SSNTD's has unraveled many applications in environmental pollution monitoring and earth sciences [1-4]. The use of advance scientific means as a non-invasive tool in studying SSNTD is becoming very important. The operation of the CR-39 SSNTD's is based on the fact that a heavy charged particle will cause extensive ionization of the material in its wake as it ionizes almost all molecules in its path. The ionized area fades along a radial path in its passage through the CR-39 SSNTD. These latent ionized path when chemically, or electrochemically etched, amplifies the ionized parts for visual (optical) assessment and possible analyses of the track parameters. There are various methods used in characterizing and counting the etched track detectors as reviewed by Nikolaev et al. [5] and Nikezic et al. [6]. Optical microscopes have been used to visualize and count tracks after etching [7-8]. The optical microscope is accurate but quite tedious with a high assessment time when minute tracks are encountered. Ho et al. [9] used atomic force microscopy (AFM) to view 3D structures of the tracks (Pits) and were able to discriminate between genuine tracks and other damages that were similar to tracks. Nikezic et al. [10] investigated the limitation of track studies using AFM. Recently, Gautier et al. [11] have developed an apparatus for fast a screening and qualitative analysis of CR-39 detectors using a simple green He–Ne laser and a high-resolution digital single-lens reflex camera as the source and imaging devices, respectively.

Eghan et al. [12] in their previous work have described an opto-digital imaging system and used Image Pro-Plus [13] software to process the image, count and record track parameters of irradiated LR-115 detectors. In this paper, the authors seek to image fission fragments and alpha tracks simultaneously on irradiated CR-39 detectors using an opto-digital imaging system. The uniqueness of the set up is that the location of the original object through the lenses simply has scale factors that are similar for all points in the image field of interest.

2. Imaging System

Two lenses (optical system) were placed such that a coherent parallel He-Ne laser beam of uniform intensity and zero phase illuminated an electrochemically-etched CR-39 detector with a complex amplitude transmittance $g_1 = (x_1, y_1)$ located in the front focal plane of lens L_1 as shown in Fig. 1. The bi-dimensional Fourier transform $G_1(u,v)$ of the object at O by L_1 has an amplitude distribution in the back focal plane of L_1 at the Fourier plane and this is expressed as [14-16]

$$G_1(u,v) = F_2[g_1(x_1, y_1)] = \int_{-\infty}^{+\infty}\int g_1(x_1, y_1)\exp(-j2\pi(ux_1 + vy_1))dx_1 dy_1 \quad (1)$$

Where, $u = x_f f_1/\lambda$ and $v = y_f f_1/\lambda$ are the rectangular spatial frequencies of the input in the Fourier plane. The beam wavelength (λ) is 0.63μm and f_1 is the focal length of the Lens L_1, which is an achromatic doublet type. The system performs a linear

* eghan_jm@yahoo.com

invariant transformation and permits signal processing. There is the possibility to manipulate the spectrum of the input image by using a mask or optical filters. The use of mask or optical filters only improves the signal to noise ratio by increasing the selectivity of the correlation process, however, it decreases the systems tolerance for signal size and orientation variations. The manipulation process results in the deformation of tracks in the image, which does not aid further processing.

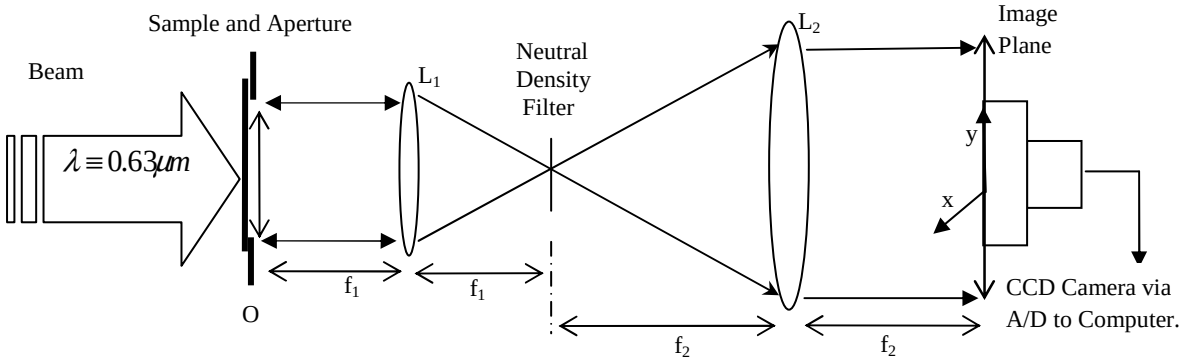

Fig.1. The optical system arrangement [12].

The second lens (L_2) has a longer focal length such that an image with higher density track can be projected. The configuration has a fixed distance dictated by the focal length of the lenses with the magnification of the image derived from the ratio of their focal lengths. Thus the optical arrangement performs an inverse Fourier transform projecting the image onto the camera with an amplitude distribution in the output plane $(g_2(x_2, y_2))$ given by [16] as

$$g_2(x_2, y_2) = F_2[G_2(u', v')] = \int_{-\infty}^{+\infty} g(Mx_1, My_1)h(x_2 - Mx_1, y_2 - My_2)dx_1 dy_1 \quad (2)$$

Where, $u' = x_f f_2 / \lambda$ and $v' = y_f f_2 / \lambda$.

The output spectrum is a convolution of the input response scaled by a magnification factor M with a point spread function impulse response $h(x_2, y_2) = F_2[H(u,v)]$. $M = f_2 / f_1$ is the lateral magnification of the imaging system and f_2 is the focal length of lens L_2. $H(u,v)$ is the transfer function at the Fourier plane. The amplitude distribution of the light intensity can be considered to include all total internally reflected individual light rays that impinge on the walls of the tracks and appear as dark shapes representing the tracks in the image.

2.1 Experimental procedure

In this work, four CR-39 SSNTD (Tastrak, Bristol, UK, 0.6% DOS plasticizer, 6.0 KeV/μm detection threshold) of size 1.5 cm^2 of thickness 0.1 cm were irradiated separately for a determined period and distance from a calibrated Califonium^{252} source. For comparison each sample was viewed with a microscope (Carl Zeiss type, 4-1000x) on a graduated mechanical stage with an adjustable illuminator, as an initial examination to get a general impression of the tracks. Another detector was kept non-irradiated and used as the control sample. Conditions for the preferential amplification (etching) of the detectors are summarized in Table 1.

Normal air was used as the medium in collimating the particles for irradiating the detector through a 4.0 mm diameter polyvinyl chloride (PVC) pipe of height 2.5 mm. The detectors were irradiated in a normal incidence mode. The expected fission track density is ~5.0 x10^2 tracks/mm^2 for an irradiated area of the detector. CR-39 detectors laterally place in the object plane O of Fig. 1. The N tracks in the CR-39 are illuminated by a low power (40% of 1mW) He-Ne laser beam. The beam is totally internally reflected by the tracks walls and consequently appears as dark gray in the image plane.

In the present investigation, the energies of incident particles at the detector surface is a function of the source-distance, which was calculated using the range and stopping power for heavy ions by Northcliffe and Schilling [17].

Table 1: Characteristics of the detectors and its preferential etching conditions.

Material			**Type of Etching**	**Etching Conditions**		
CR-39	Density ($g\ cm^{-3}$)	Refractive Index	Electro-chemical	70°C	Time h^{-1}	$V_b\ \mu m\ h^{-1}$
Ally diglycol--carbonate	1.32	1.45	4.5 kV	$NaOH_{(aq)}$ 6.0 N	7.0	0.22

2.2 Data processing and analysis

The images were captured frame per frame and saved as TIF File using the Image-Pro Plus [13]. For each detector two fields of view (each 0.03 cm^2) were captured taking into account track densities so as to achieve an error less than 5%. To analyse the tracks, the following process were adhere to in order to calibrate and identify the tracks:

1. *Calibration*: A series of pseudo opaque circular spots (Perspex dots) of diameter in the range 2 - 30 μm (measurement obtained from the microscope) were imaged. These values were stored in the calibration module of the Image Pro software by locating the vertical and horizontal length in pixels of each spot. The software pixels gray levels have been designed to fit any scale of the coordinate system in the image. This allows one to extract information of any physical parameter.
2. *Processing*: The spatial resolution of the recorded image corresponds to 0 to 255 gray levels. A background image of the laser beam through the non-irradiated electrochemically etched detector was imaged and subtracted from each image of an irradiate detector to eliminate some background noise. The images were enhanced by sharpening, using a *3x3 convolution with 2 passe*s and a Gaussian filter with a *3x3, with 1 pass*.
3. *Counts/Analysis*: To recognize the damages and defects, a different gray scale range on the average, other than (0 - 82), and aspect ratio within 1.0 - 1.75, identified the tracks. This gave an adequate distinction of the tracks from the damages. A size constrain of area < 28 μm^2 for alpha tracks and > 28 μm^2 for the Fission tracks were invoked and used simultaneously with the gray scale range to count separately the two types of tracks.

With the calibration condition set, the software draws a horizontal line at the central pixels of each track as shown in Fig. 2. The line M_1M_2rotates in a 2° step clockwise direction and an average of this is taken as the average diameter.

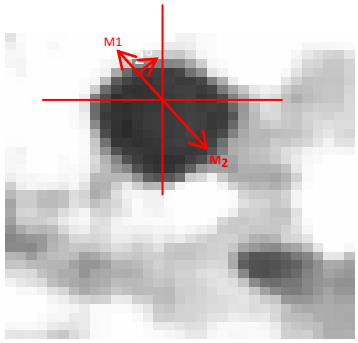

Fig.2. A schematic illustration of how the software measures the diameter of an arbitrary etched track, in a 2° step clockwise rotation.

The output of the track analysis using the Image-Pro plus on the processed digitized image provided the following on each track: a number associated to a counted track, classification of tracks according to track aspect ratio (i.e., ratio of major to minor axis that gives the circular or ellipsoidal nature of the track) and area. The software has a Dynamic Data Exchange (DDE) with Microsoft Excel Program, enabling the track parameter data to be graphically represented.

3. Results and Discussion

Results generated using the "Image Pro" application of classification are shown in Figs. 3a, 3b and 4a for counted alpha and fission fragments tracks, respectively. Tracks that remain visible after processing are efficiently classified, counted and the area simultaneously recorded. Border tracks are ignored so as not to have a false data since the complete size is unknown. Figs. 3c and 3d, and Figs. 4b and 4c, show statistical information on tracks aspect ratio and area distribution of the two tracks types, respectively.

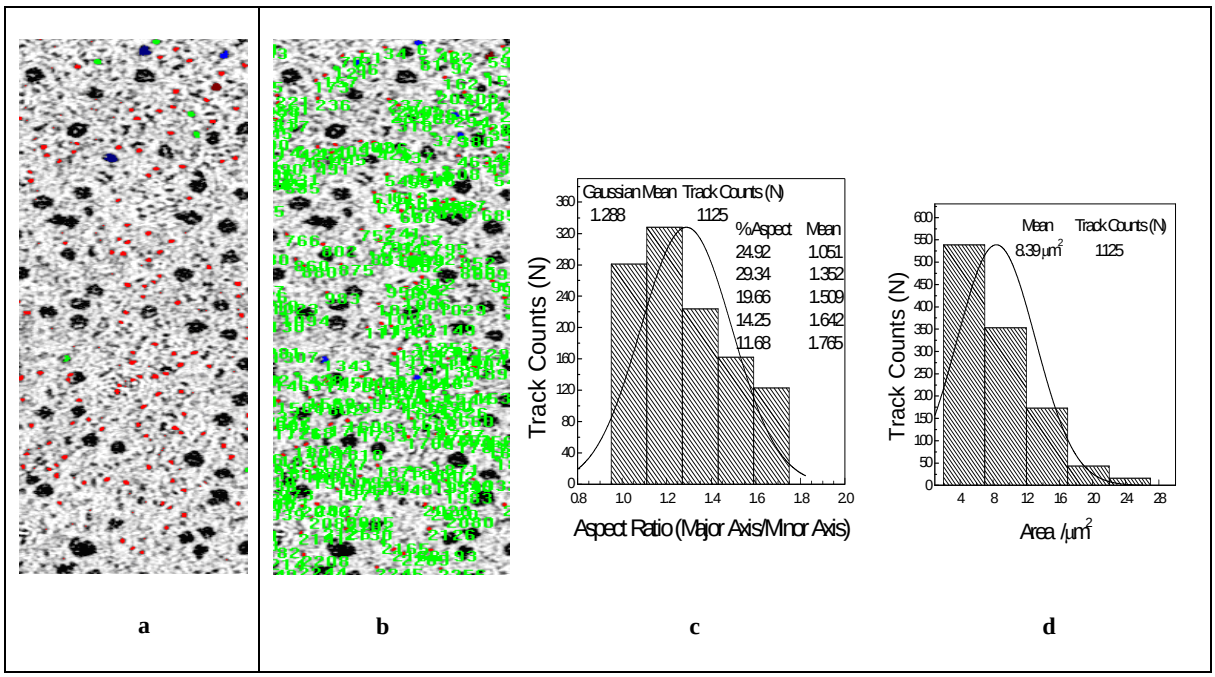

Fig. 3. (a) A section of captured CR-39 (CIII) detector with 5 classifications of alpha tracks. (b) CIII with only alpha tracks counted and associated with a number. (c) Histogram depicting the area classification with a Gaussian fit and their percentage means. (d) A histogram on class distribution of its Aspect ratios with a Gaussian fit.

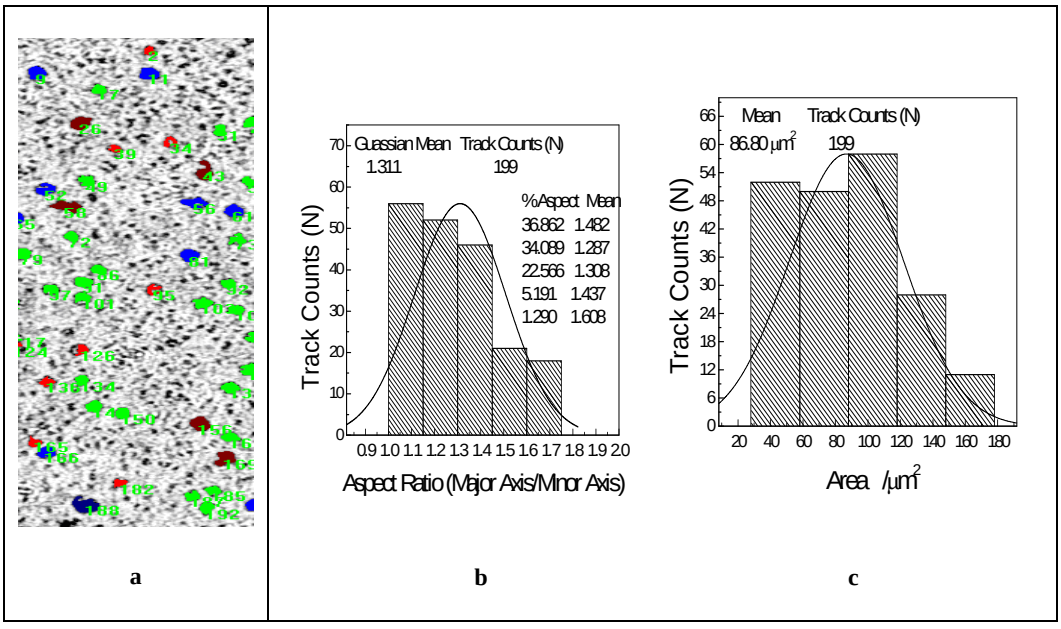

Fig.4. (a) A section of CIII classified and counted Fission fragments with numbers associated. (b) A histogram on class distribution of its Aspect ratios with a Gaussian fit. (c) Histogram depicting the Area classification with a Gaussian fit and their percentage means.

Table 2 summarizes the track distribution on the four detectors. A standard deviation of 0.01 and 0.06 % for the area of alpha and fission tracks, respectively, were obtained. The standard deviation for their aspect ratio was 0.004% for alpha tracks and 0.01% for fission tracks.

Table 2: A table showing the mean area and aspect ratio values of each CR-39.

	Alpha (α)		Fission Fragments		
Detectors	Mean track area / μm^2	Mean aspect Ratio	Mean Track area / μm^2	Mean aspect Ratio	Total Counts
CI	8.38	1.286	86.78	1.341	2660
CII	8.38	1.278	86.67	1.302	2656
CIII	8.39	1.288	86.80	1.311	2658
CIV	8.36	1.286	86.82	1.309	2656

The results in Table 2 emphasize the fact that the detectors had similar tracks parameters as they were irradiated from the same source and preferential etching conditions.

Figs. 5a-5b show the relationship between track area and particle energy. The graphs show a decrease in energy with increasing area of tracks as proposed by Khayrat and Durrani [18] and Hofy et al. [19]. Thus the size of an etched track is a measure of the total energy deposited in the medium. The results further confirm the versatility of the system and its efficiency and reliability. The selection of the optical configuration makes it possible to view the two types of tracks which are unique. This is not found in most track imaging systems as most configuration views or images only one range of track set at a time. The large area viewed ($0.03cm^2$) is much greater than the microscope.

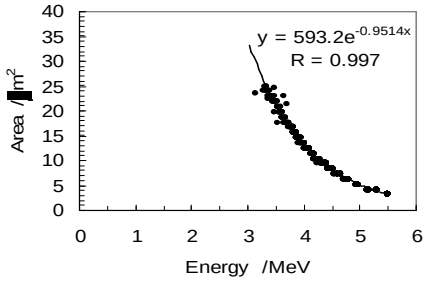

(a)

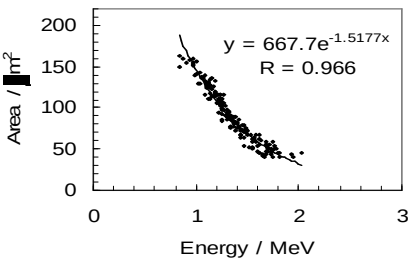

(b)

Fig.5. A plot of area versus residual energy of tracks for: (a) alpha tracks and (b) fission fragments.

4. Conclusion

An alternative image technique and counting of nuclear tracks induced in CR-39 has been developed. Counting and track parameter evaluation was fast (2 s per image frame) and the configuration enables the imaging of the two types of particle tracks. The authors are aware of AFM, and other automatic or semi-automatic imaging and counting systems [20] developed, but they are complex and expensive. An improvement on our system would be to reduce the cost by using a digital camera and an open source imaging software.

Acknowledgments

The authors wish to thank the Abdus Salam International Centre for Theoretical Physics (ICTP), Trieste, Italy for the financial contributions towards the development of science through their affiliated center LAFOC, UCC. Moses J. Eghan is grateful to the Associate Scheme of ICTP for their financial support during his stay at the Centre and the use of the library and other facilities to write this paper. The authors are grateful to Ghana Atomic Energy Commission (GAEC) for providing the detectors and the sources for this work.

References

[1] D. Amarni and M. Belgaid, Radiation Physics and Chemistry **61**, 639 (2001).

[2] *Applications in Radiation Protection, Earth Sciences and the Environment*, edited by S. A. Durrani and R. Ilic (World Scientific Singapore, 1997).

[3] M. E. Moore, H. J. Gepford, R. E. Hermes, N. E. Hertel and R. T. Devine, Rad. Prot. Dos. **101**, 43 (2002).

[4] P. Wanabongse, B. Sola, J. Jamsangtong and S. Rattanabussayaporn, Indian Journal of Physics **83**, 6 (2009)

[5] V. A. Nikolaev and R. Ilic, Rad. Measurements, and references therein **30**, 1 (1999).
[6] D. Nikezic and K. N. Yu, Materials Sc. and Engineering, and references therein **46**, 51 (2004).
[7] H. Arias D. Palacios, L. Sajo-Bohus and T. Vilora, Rad. Measurements **40**, 357 (2005).
[8] N. Petford, D. Wertheim and J. A. Miller, Journal of Microscopy **217**, 179 (2005).
[9] J. P. Y. Ho, C. W. Y. Yip, D. Nikezic and K. N. Yu, Rad. Measurements **36**, 155 (2003).
[10] D. Nikezic et al., Rad. Measurements (2002).
[11] D. C. Gautier, J. L. Kline, K. A. Flippo, S. A. Gaillard, S. A. Letzring and B. M. Hegelich, Rev. Scientific Instruments **79**, 10e536 (2008).
[12] M. J. Eghan, P. K. Buah-Bassuah and O. C. Oppon, Meas. Sci. Technol. **18**(11), 3651 (2007).
[13] Media Cybernetics, Image Pro-Plus version 5.0 for Windows, Reference Guide, The Proven Solution for Image Analysis 480 (2000).
[14] H. Stark, *Theory and Applications of Optics Fourier Transforms* (Academic Press, 1982) p.12.
[15] J. W. Goodman, *Introduction to Fourier Optics* (McGraw-Hill Inc., 2nd Edition, New York, 1996) Chapters 2 and 5.
[16] S. P. Almeida and G. Indebetouw *Applications of Optical Fourier Transforms*, Ed. H. Stark (Academic Press, 1982) p.46.
[17] L. C. Northcliffe and R. F. Schilling, Nuclear Data Tables **A7** Range and Stopping Power Tables for Heavy ions. OD94, 233 (1970).
[18] A. H. Khayrat and S. A. Durrani, Rad. Measurements **30**, 15 (1999).
[19] M. El Hofy, H. El Samman and W. Arafa, Rad. Measurements **31**, 217 (1999).
[20] C. Vazquez-Lopez, B. E. Zendejas-Leal, J. S. Bogard, J. I. Golzarri and G. Espinosa, Rad. Measurements **44**, 791 (2009) and references therein.

Received: 24 February, 2011
Accepted: 4 April, 2011